Dissolution swelling effect-assisted interfacial morphology refinement enables high efficiency all-polymer solar cells

Weichao Zhang[a,b,#], *Yaochang Yue*[a,#] , *Fei Han*[c,#], *Hong Zhang*[b]*, *Yongqing Wang*[a], *Shengli Yue*[a], *Bohao Song*[d], *Guanghan Zhao*[b], *Chao Qu*[a], *Rongshen Yang*[a], *Rui Zeng*[c], *Shilin Li*[a], *Chuanyun Li*[b], *Jin Zhou*[b], *Guanghao Lu*[d], *Wanfei Shi*[b], *Xuning Zhang*[e], *Feng Liu*[c],*Ming Zhang*[c]*, *Huiqiong Zhou*[b]* *and Yuan Zhang*[a]*

[a]School of Chemistry, Beijing Advanced Innovation Center for Biomedical Engineering, Beihang University, Beijing 100191, People's Republic of China.
[b]CAS Center for Excellence in Nanoscience, National Center for Nanoscience and Technology, Beijing 100190, P. R. China.
[c]Frontiers Science Center for Transformative Molecules, In-situ Center for Physical Science, and Center of Hydrogen Science, School of Chemistry and Chemical Engineering, Shanghai Jiao Tong University, Shanghai 200240, China.
[d]Frontier Institute of Science and Technology, Xi'an Jiaotong University Xi'an, 710054, China.
[e]College of Physics Science & Technology, Hebei University, 071000, China.
[#]These authors contributed equally: Weichao Zhang, Yaochang Yue and Fei Han.

Experiments

Materials: PM6, BTA3, PCBM, ITIC, IT-4F, IT-M and PY-IT were purchased from Solarmer Company and Nanjing Zhiyan Technology Co.， Ltd. PNDIT-F3N was purchased from eFlexPV Limited (China). deionized water was used in our experiments. PEDOT:PSS was purchased from Heraeus (CLEVIOSTM PVP Al 4083). Cholorform (CF) was purchased from Sigma-Aldrich. All reagents were purchased from Sigma-Aldrich, Acros, Alfa Aesar or TCI and used as received.

Gaussian Calculations: Density functional theory (DFT) calculations were performed using the Gaussian 09 program with the B3LYP exchange-correlation functional. All-electron triple-ξ valence basis sets with polarization functions (6-31G (d, p)) are used for all atoms. Geometry optimizations were performed with full relaxation of all atoms. For each molecule, various conformations with different dihedral angles were optimized, and the data for the one with the lowest energy were reported.

Device fabrication: The solar cells in this study were fabricated using a conventional coated glass substrates were pre-cleaned sequentially with detergent, deionized water, CMOS grade acetone, and isopropanol for 25 minutes, followed by drying with nitrogen gas, and then treated with UV-ozone for 20 minutes before use. PEDOT:PSS was spin-coated onto the cleaned ITO substrates at 4000 rpm for 30 s, then transferred to an oven and dried at 150°C for 20 minutes. Subsequently, the substrates were transferred to a glove box in a nitrogen atmosphere. The active layer solutions of PM6, PM6+BTA3 and PY-IT were dissolved in chloroform (CF), respectively. The active layer solution was magnetically stirred on a hot plate at 50°C for 2 hours. For PM6/PY-IT (1/1.2) type LBL devices, the PM6 donor layer from a 7.3 mg/mL chloroform solution was spin-coated at 2000 rpm for 40 seconds, followed by spin-coating the PY-IT acceptor layer from an 8.7 mg/mL chloroform solution (with 15 mg/mL DIB) at 3500 rpm for 35 seconds. Next, the devices were placed in a transition chamber and vacuumed for 5 minutes, and then annealed at 80 °C for 10 minutes in a CS_2 solvent atmosphere. For PM6+BTA3/PY-IT (1+0.05/1.2) type LBL devices, aside from adding 0.05 mass ratio of BTA3 to PM6, the preparation conditions are the same as those for PM6/PY-IT. The active layer solution was spin-coated onto PEDOT:PSS at 4000 rpm for 20 s. Then, 0.5 mg/mL PNDIT-F3Br solution was spin-coated. Finally, a 100 nm Ag electrode was evaporated. The effective area of the device is 4 mm^2.

Device characterization: The solar cell devices were characterized in a nitrogen atmosphere under the illumination of a simulated AM 1.5G (AAA grade, XES-70S1) light source. The illumination intensity in front of the cell sample was calibrated to 100 mW/cm^2 using a reference silicon cell. The current density-voltage (*J-V*) measurements of the devices were recorded along the forward scan direction from -0.1 V to 1.2 V using a computer-controlled Keithley 2400 Source Measure Unit. The EQE measurements were performed with the as-fabricated solar cell in air using a QE-R3011 instrument (Enli Technology Co. Ltd., Taiwan). The thickness of the solid films was measured using a Dektak Profilometer. The AFM images were recorded using a Bruker

multimode8 AFM. All the blend films were fabricated under optimal conditions. EQE_{EL} measurements were conducted using a homemade setup, employing a Keithley 2400 for current injection into the solar cells. Emission photon flux from the solar cells was recorded using a Si detector (Hamamatsu s1337-1010BQ) and a Keithley 6482 picoammeter. Transient photocurrent (TPC) and photovoltage (TPV) measurements were conducted on a Molex 180081-4320 under light intensity approximately equivalent to 0.5 sun. Voltage and current dynamics were recorded using a digital oscilloscope (Tektronix MDO4104C). Voltages at open circuit and currents under short circuit conditions were measured across a 1 MΩ and a 50 Ω resistor, respectively. Contact angle tests were conducted using the Drop Shape Analyzer (DSA100, KRÜSS) in static mode at room temperature. The surface free energy of each film was obtained by fitting. Specifically, the contact angle was calculated by averaging the left and right angles of a sessile drop, measured by the KRÜSS software using the tangential method. Deionized water and diiodomethane (1.5 μL) were dropped onto Si/SiO_2 wafers with the neat film, and the droplet was photographed after reaching equilibrium at the gas-liquid-solid interface. The contact angle was maintained within a standard deviation of ±1°.

Optical spectroscopy measurements: Solid thin films of polymer donor polymer and acceptor used for the absorption and fluorescence spectroscopy were prepared by spin-coating the solutions of donor or acceptor compounds pre-solubilized in chloroform (10 mg/mL) on quartz glass substrates. All the blend films were prepared following the optimal conditions for the preparation of solar cells. The absorption spectrum was measured on a Hitachi U-3010 UV-visible spectrophotometer, and the fluorescence spectroscopy was performed on a Hitachi F-7000 spectrophotometer. These optical spectroscopic tests were carried out at room temperature.

Measurements of electron and hole mobilities by the space charge-limited current (SCLC) method: The hole-only and electron-only The electron-only devices were

fabricated with a configuration of ITO/titanium (diisopropoxide) bis(2,4-pentanedionate) (TIPD)/active layer/PDINO/Al and hole only devices were configured with ITO/PEDOT:PSS/active layer/ Ag. The TIPD buffer layer was prepared by spin-coating a 3.5 wt % TIPD isopropanol solution onto the pre-cleaned ITO substrate and then baked at 150 °C for 10 min to convert TIPD into TOPD. Subsequently, the blend was spin-coated on the TOPD-coated substrates under the same condition as used for solar cell. Finally, an Al layer was thermally deposited on the top of the blend in vacuum (deposition speed of 1 Å/s). The electron mobility was extracted by fitting the current density–voltage curves using the Mott–Gurney law $J = 9\varepsilon\varepsilon_0\mu V^2/8L^3$, where ε is the dielectric constant of the organic component, ε_0 is the permittivity of the vacuum (8.85419×10^{-12} $CV^{-1}m^{-1}$), μ is the zero-field mobility, J is the current density, L is the thickness of the active layer, and $V = V_{app} - V_{bi}$, here V_{app} is the applied potential, and V_{bi} the built-in potential which results from the difference in the work function values of the cathode. From the plot of $J^{1/2}$ versus V, the hole and electron mobilities can be deduced.

GIWAXS measurements: The GIWAXS data were collected at the Xeuss 2.0 SAXS/WAXS laboratory beamline using a Cu X-ray source (8.05 keV, 1.54 Å) and a Pilatus3R 300K detector. The incident angle was 0.15°. The preparation conditions of the mixed films were optimized for the highest efficiency devices (annealing temperature ranged from 288 K to 363 K). All GIWAXS characterizations in this study were conducted at the Institute of High Energy Physics, Chinese Academy of Sciences.

In-situ ultraviolet-visible (UV-vis) absorption measurements: In-situ UV-vis absorption spectra were recorded using a Filmetrics F20-EXR spectrometer in transmission mode, with a resolution of 0.04 seconds. The spectrometer consists of a light source and a detector, which are fixed above and below the substrate, respectively, and aligned along the same vertical line. During the coating process, the detector collected the transmission spectra ranging from 400 to 1000 nanometers. The UV-vis

absorption spectra were calculated using the equation $\Delta\lambda$ = -log10(T), where $\Delta\lambda$ represents the absorbance at a specific wavelength (λ), and T is the calculated transmittance. The light source and detector were turned on before coating the film, so the time zero corresponds to when the detector collected the first transmission spectrum of the solution. Prior to time zero, only noise was present in the transmission spectra.

In-situ photoluminescence spectroscopic measurements: The in-situ photoluminescence spectrum measurement was conducted using a laser device (MGL-III-785-300mW BH81223), with an excitation wavelength of 445 nanometers.

Energy loss analysis

Fourier-transform photocurrent spectroscopy-external quantum efficiency (FTPS-EQE) was measured using an integrated system (PECT-600, Enlitech). External electroluminescence quantum efficiency (EQE_{EL}) measurements were performed by applying external voltage/current sources through the devices (REPS, Enlitech). The total energy loss (ΔE) can be separated into three parts:

$$\Delta E_{loss} = qE_g - V_{OC} = \left(E_g - qV_{OC}^{SQ}\right) + \left(qV_{OC}^{SQ} - qV_{OC}^{rad}\right) + \left(qV_{OC}^{rad} - qV_{OC}\right) = \Delta E_1 + \Delta E_2 + \Delta E_3 \quad (1)$$

Among them, $\Delta E_1 = (E_g - qV_{OC}^{SQ})$, from the radiative recombination loss above the E_g, is unavoidable in all types of solar cells and it can be determined based on the energy gap of solar cells. The second part, $\Delta E_2 = (qV_{OC}^{SQ} - qV_{OC}^{rad})$, stems from the radiative recombination loss below the bandgap, where the ΔV_{OC}^{rad} can be calculated by realistic radiative recombination using a reciprocity relation between FTPS-EQE and EQE_{EL}. According to the estimated equation, the third loss part, ΔE_3 can be determined with the relation $\Delta E_3 = (qV_{OC}^{rad} - qV_{OC})$.

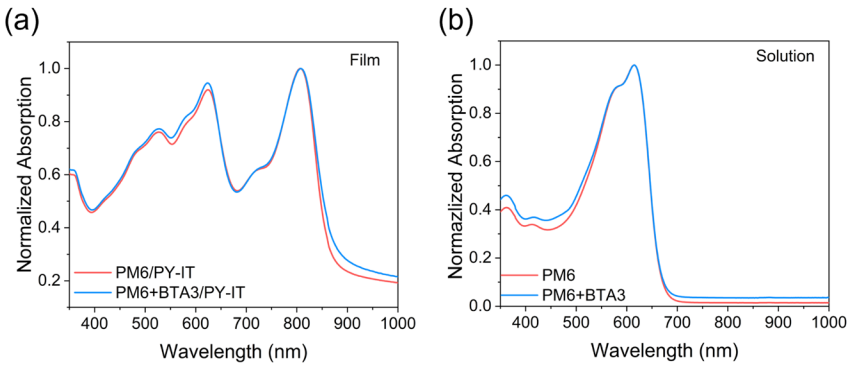

Figure S1. Steady-state absorption spectra measured on the blends of PM6/PY-IT and PM6+BTA3/PY-IT. (a) Solid-state films; (b) in solution. The ratio of PM6:BTA3 is 1:0.05.

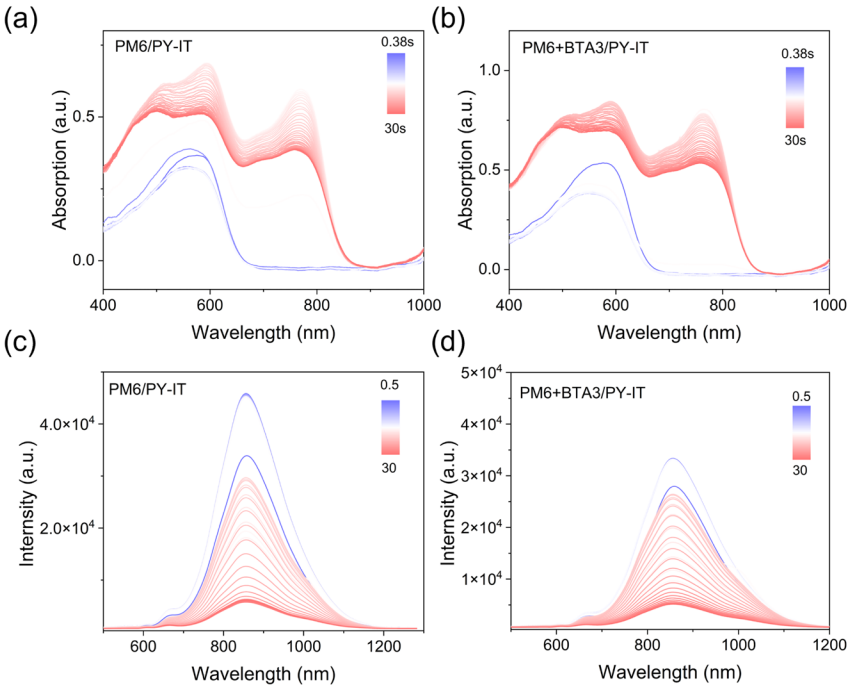

Figure S2. In-situ UV-Vis absorption spectra of (a) PM6/PY-IT and (b) PM6+BTA3/PY-IT blend films; In-situ PL spectra of (c) PM6/PY-IT and (d) PM6+BTA3/PY-IT blend films.

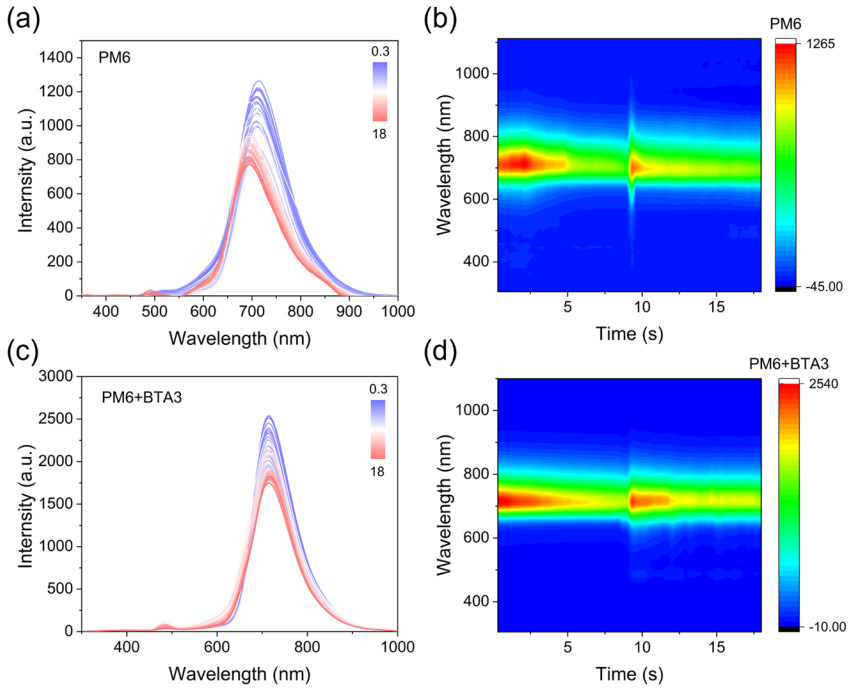

Figure S3. In-situ PL spectra (a, c) and 2D color plots (b, d) based on the samples of (a) pure PM6 and (c) PM6+BTA3.

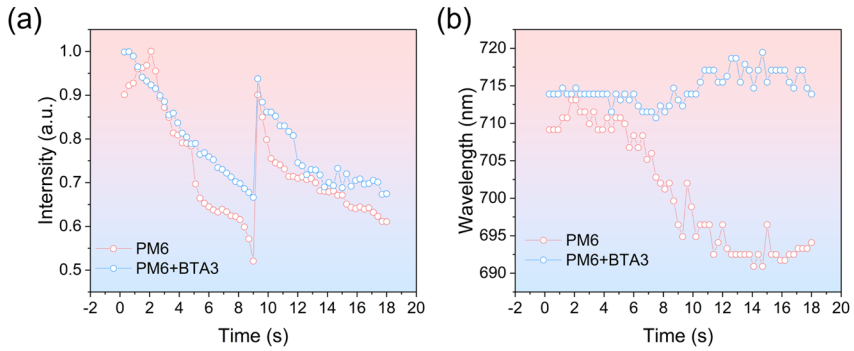

Figure S4. Time evolution of the PL intensity (a) and PL peak location (b) extracted from the in-situ PL spectroscopy measured on PM6/PY-IT and PM6+BTA3/PY-IT samples.

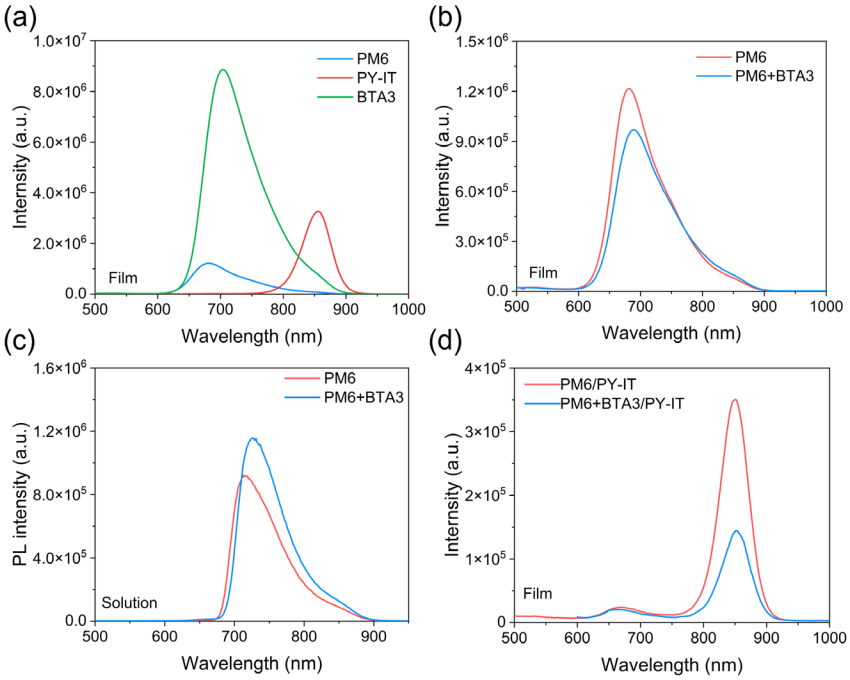

Figure S5. Steady-state PL spectra of (a) neat PM6, BTA3 and PY-IT films, (b) PM6 and PM6+BTA3, (c) PM6 and PM6+BTA3 (Solution) and (d) PM6/PY-IT and PM6+BTA3/PY-IT. The ratio of PM6: BTA3 is 1:0.05.

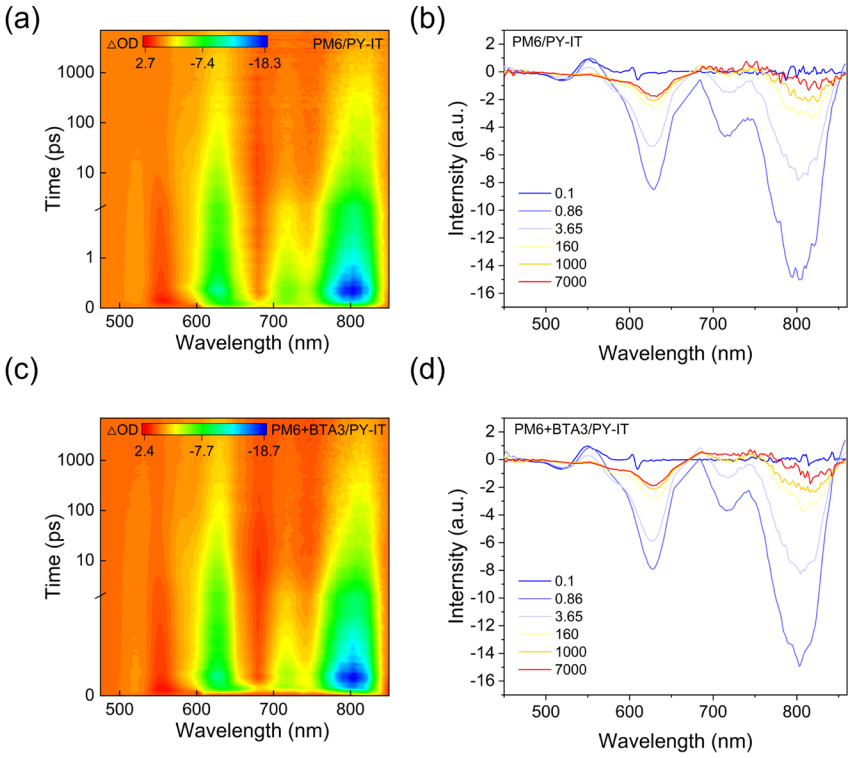

Figure S6. (a, c) Two-dimensional color maps of ps-transient absorption (ps-TA) spectra based on PM6/PY-IT and PM6+BTA3/PY-IT films at specified delay times

under 800 nm excitation. (b, d) TA spectra of PM6/PY-IT and PM6+BTA3/PY-IT films under 800 nm excitation.

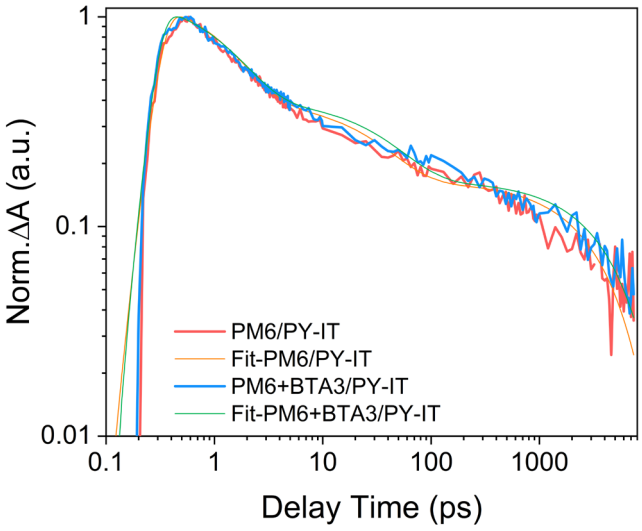

Figure S7. TA decay kinetics measured on the various pPHJ films.

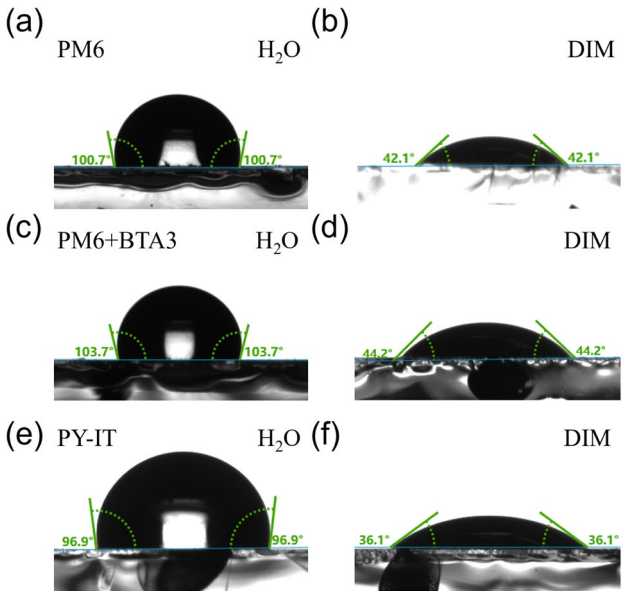

Figure S8. Snapshots of contact measurements based on (a, b) neat PM6, (c, d) PM6+BTA3 and (e, f) neat PY-IT used to determine the Flory-Huggins interaction parameter.

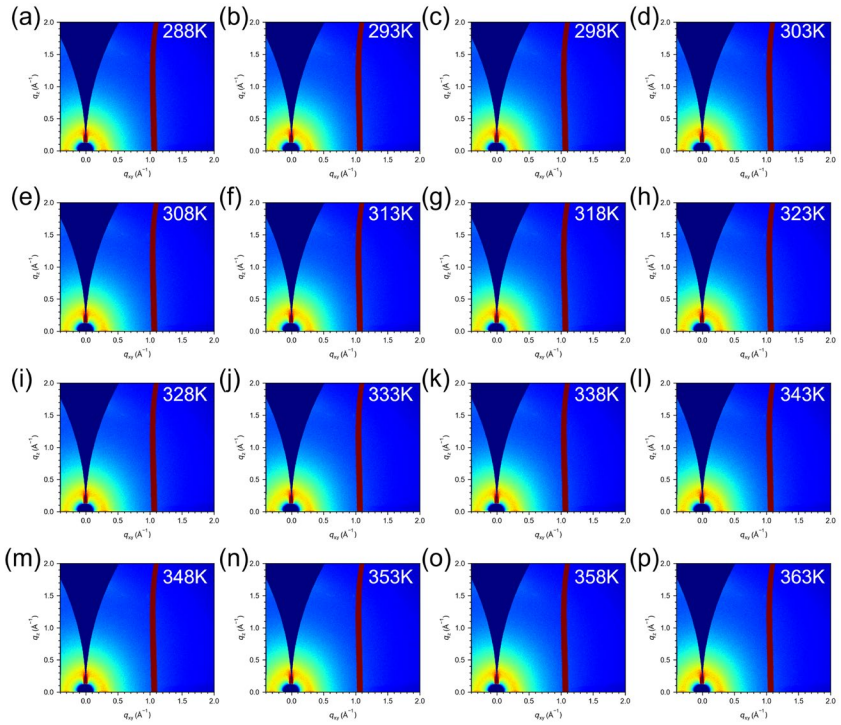

Figure S9. In-situ 2D GIWAXS patterns with thermal annealing based on the PM6/PY-IT film.

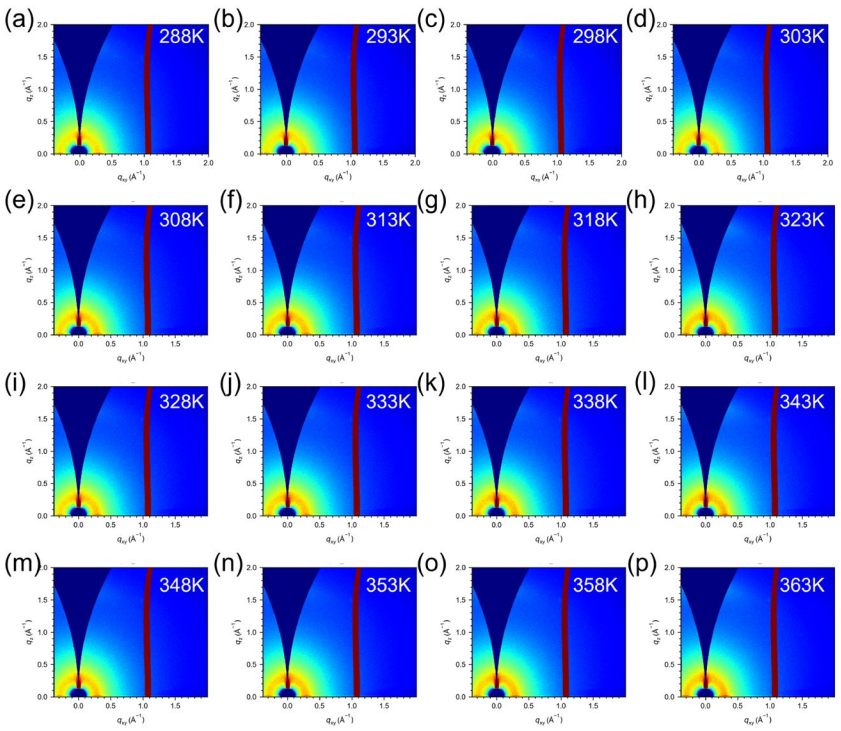

Figure S10. In-situ 2D GIWAXS patterns with thermal annealing based on the PM6+BTA3/PY-IT film.

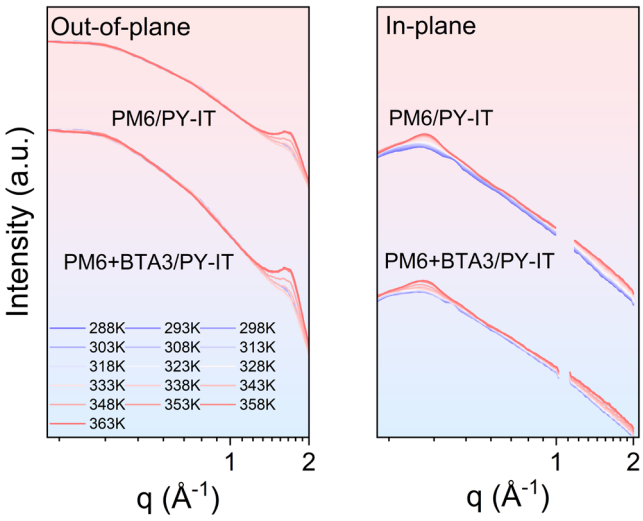

Figure S11. line-cut profile curves extracted from in-situ GIWAXS patterns with thermal annealing based on PM6/PY-IT and PM6+BTA3/PY-IT films.

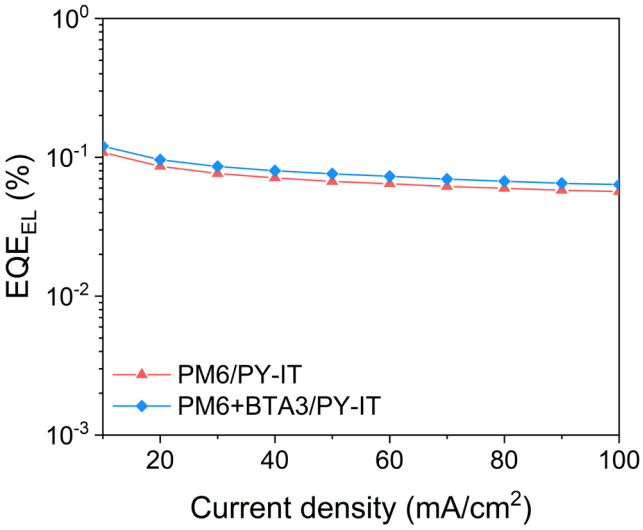

Figure S12. Electroluminescence quantum efficiency (EQE_{EL}) as a function of injected current density measured on PM6/PY-IT and PM6+BTA3/PY-IT solar cells.

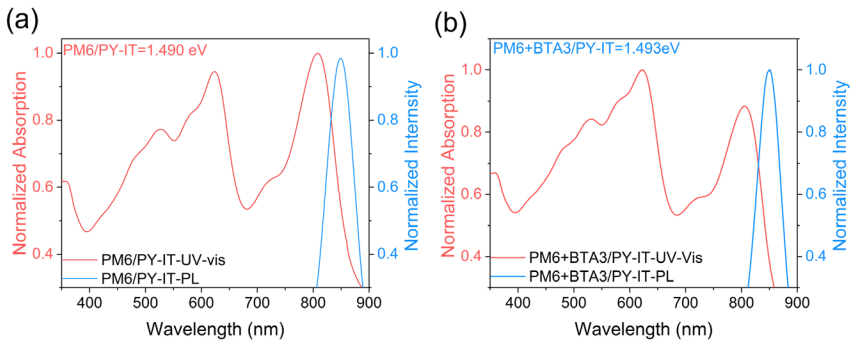

Figure S13. The bandgap values are calculated from the intersection of absorption and fluorescence, as shown in the figure: (a) PM6/PY-IT; (b) PM6+BTA3/PY-IT.

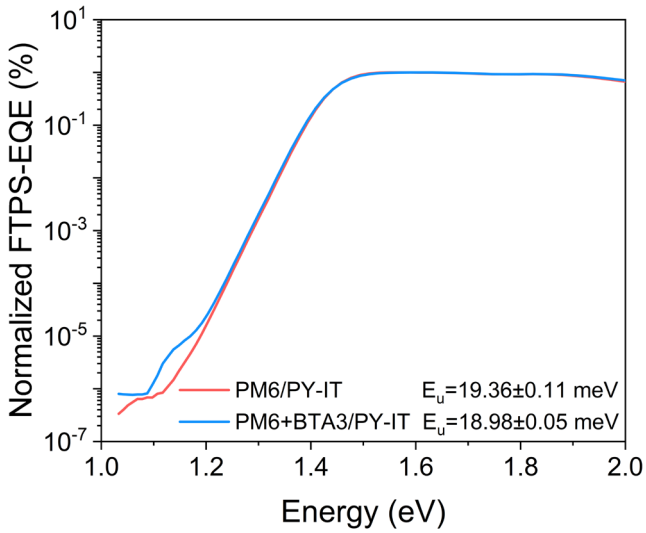

Figure S14. Normalized Fourier Transform Photocurrent Spectroscopy (FTPS) measurement results.

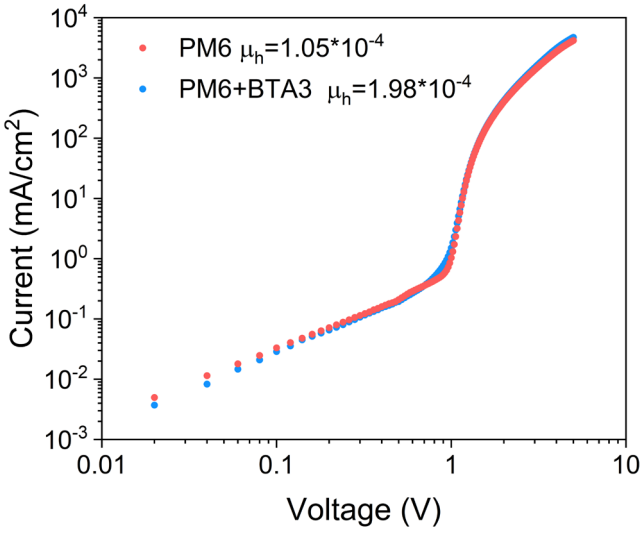

Figure S15. Dark *J*–*V* plots of hole-only devices based on the active layers of PM6/PY-IT and PM6+BTA3/PY-IT.

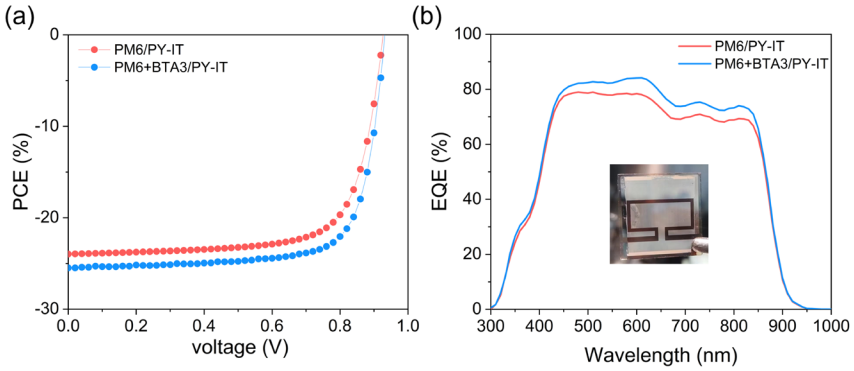

Figure S16. (a) *J*-*V* curves and (b) EQE spectra of PM6/PY-IT and PM6+BTA3/PY-IT solar cells with large device area (1 cm^2). Also shown in (b) is the photo of an actual large-area device.

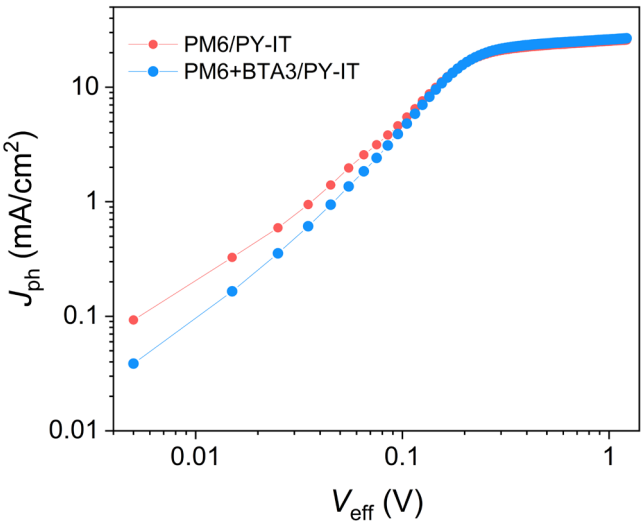

Figure S17. J_{ph} versus V_{eff} characteristics of the PM6/PY-IT and PM6+BTA3/PY-IT devices.

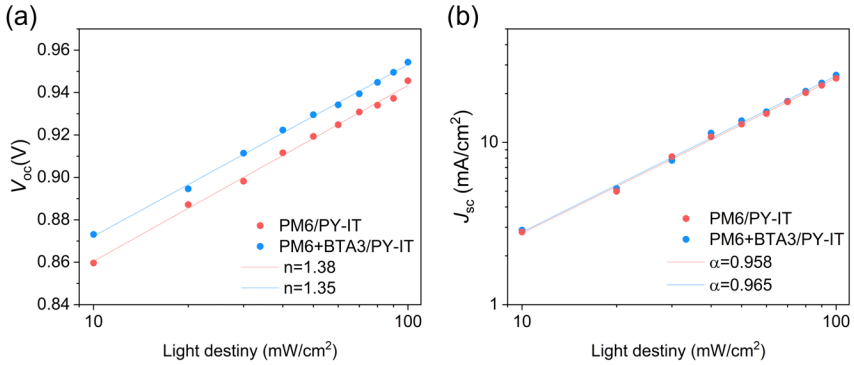

Figure S18. (a) Plots of V_{oc} versus light intensity and (b) J_{sc} versus light intensity based on PM6/PY-IT and PM6+BTA3/PY-IT.

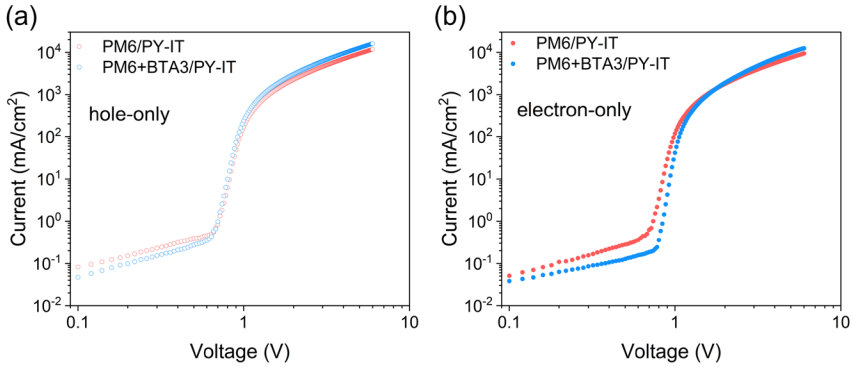

Figure S19. Dark *J*–*V* curves of single-carrier devices based on PM6/PY-IT and PM6+BTA3/PY-IT.

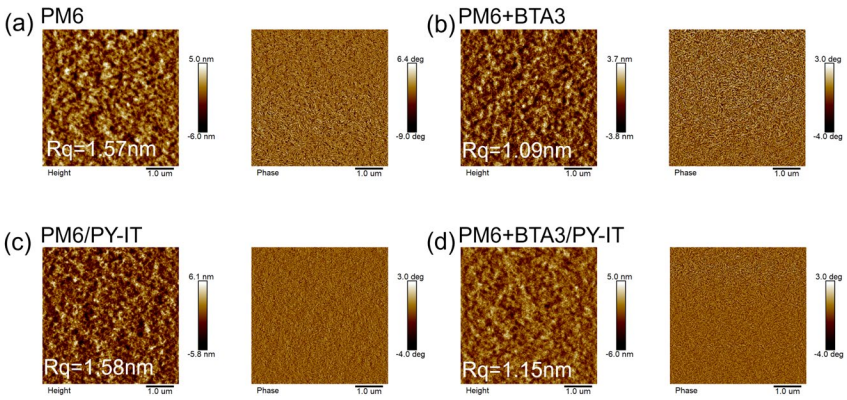

Figure S20. Atomic force microscopy topographic and phase images based on thin films of (a) neat PM6, (b) PM6+BTA3 blend, (c) PM6/PY-IT blend and (d) PM6+BTA3/PY-IT blend.

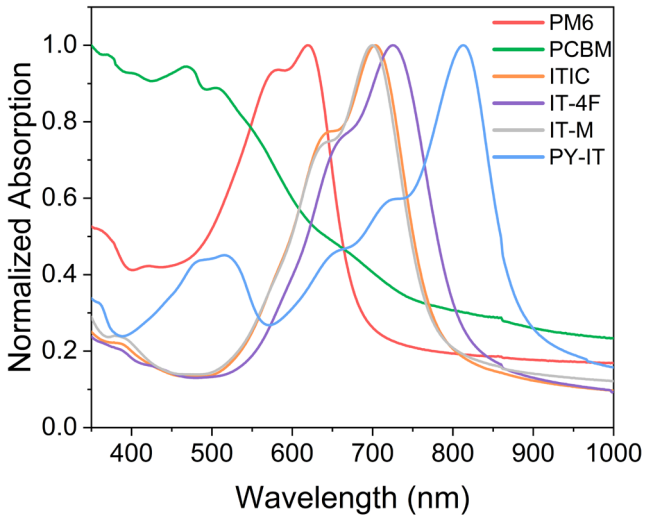

Figure S21. Steady-state absorption spectra were measured on pure films of PM6, PCBM, ITIC, IT-4F, IT-M and PY-IT.

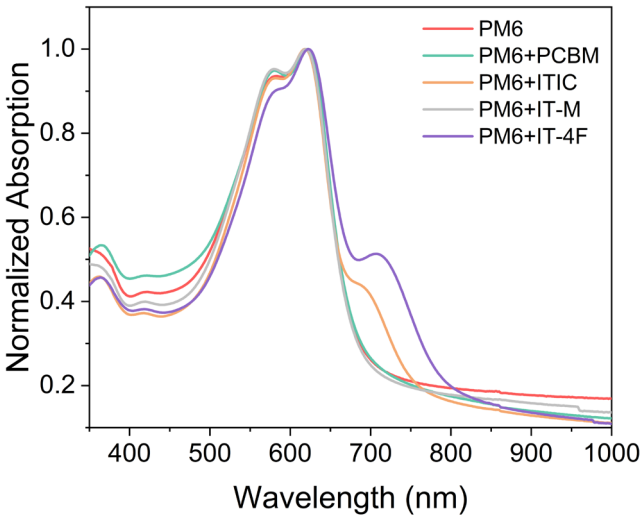

Figure S22. Steady-state absorption spectra based on PM6, PM6+PCBM, PM6+ITIC, PM6+IT-M and PM6+IT-4F films.

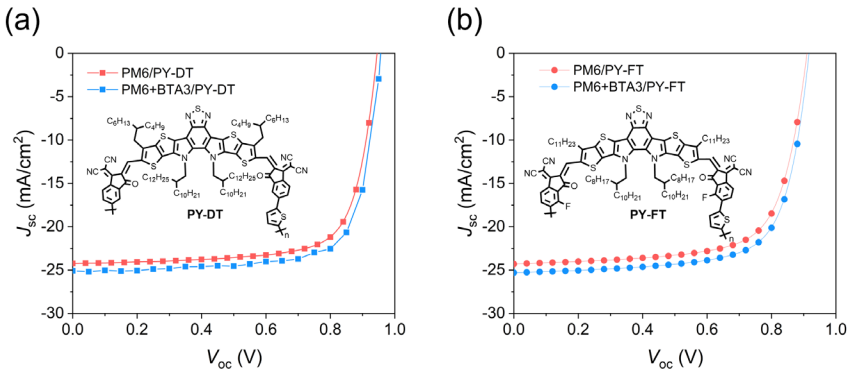

Figure S23. The improvement in device efficiency after introducing BTA3 into (a) PM6/PY-DT and (b) PM6/PY-FT.

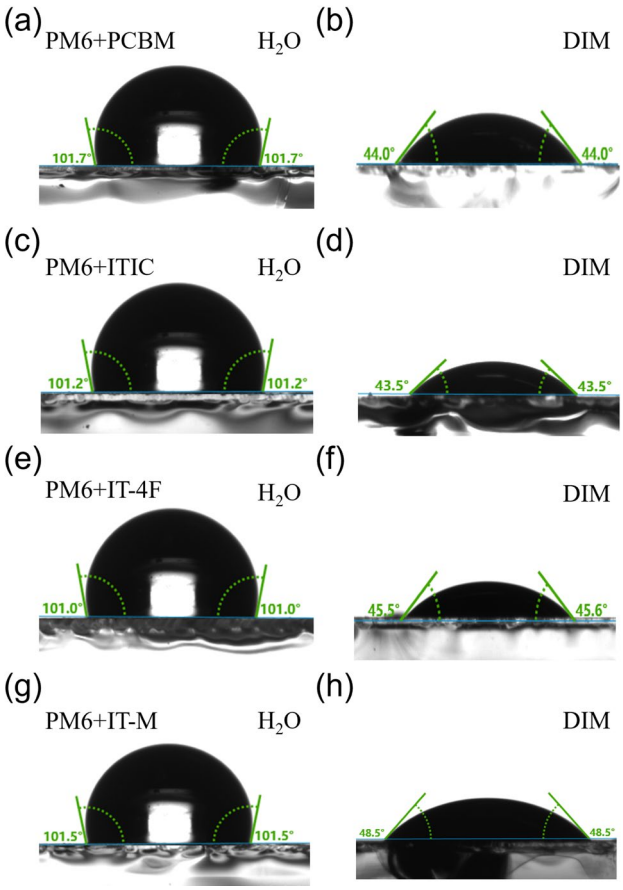

Figure S24. Snapshots of contact angle measurements based on (a, b) PM6+PCBM, (c, d) PM6+ITIC, (e, f) PM6+IT-4F and (g, h) PM6+IT-M used to determine the Flory-Huggins interaction parameter.

Table S1. Contact angles (θ), surface energy (γ), and Flory-Huggins interaction parameters ($\chi_{donor-acceptor}$) determined for PM6, PM6+BTA3 and PY-IT.

Active layer	θ_{Water} [deg.]	$\theta_{dilldomethane}$ [deg.]	γ [Mn m^{-1}]	χ_{D-A}
PM6	100.7	42.1	38.55	0.06
PM6+BTA3	103.7	44.2	37.45	0.11
PY-IT	96.9	36.1	41.59	/

Table S2. Crystal correlation length (CCL) values in the in-plane and out-of-plane directions determined on PM6/PY-IT and PM6+BTA3/PY-IT films at different annealing temperatures.

	PM6/PY-IT		PM6+BTA3/PY-IT	
Annealing	Ip plane CCL (Å)	Out of plane CCL (Å)	Ip plane CCL (Å)	Out of plane CCL (Å)
288	27.54	2.09	50.81	1.50
293	28.35	2.11	50.99	1.86
298	29.06	2.14	51.05	1.97
303	30.18	2.16	51.26	2.68
308	31.76	2.21	51.58	3.87
313	33.58	2.25	51.85	4.53
318	34.64	2.31	52.06	5.86
323	36.03	2.34	52.37	6.49
328	39.13	2.38	52.68	7.84
333	41.25	2.43	52.89	8.78
338	43.42	2.48	53.18	9.75
343	44.63	2.53	53.51	10.83
348	45.85	2.61	53.85	13.94
353	46.34	2.75	54.27	16.19
358	47.12	2.92	55.28	18.33
363	46.81	3.11	55.89	22.35

Table S3. Detailed energy losses determined on different OSCs.

Active layer	E_{gap} (eV)	qV_{OC}^{SQ} (eV)	ΔE_1 (eV)	ΔE_2 (eV)	ΔE_3 (eV)[a]	E_{loss} (eV)
PM6/PY-IT	1.490	1.231	0.259	0.117	0.183	0.559
PM6+BTA3/ PY-IT	1.493	1.234	0.259	0.111	0.180	0.550

a)ΔE_1: Above-bandgap radiative recombination loss; ΔE_2: below-bandgap radiative recombination loss; ΔE_3: nonradiative recombination loss.

Table S4. Summarized photovoltaic parameters of large-area (active area of 1 cm^2) OSCs based on PM6/PY-IT and PM6+BTA3/PY-IT under AM 1.5G (100 mW/cm^2) illumination (average PCE obtained from at least 10 devices).

Active layer	V_{oc} (V)	J_{sc} ($mA \cdot cm^{-2}$)	Cal. J_{sc}[a] ($mA \cdot cm^{-2}$)	FF (%)	PCE (%)
PM6/PY-IT	0.927	23.97	22.43	72.19	16.04
	0.925±0.003	23.78±0.24		71.89±0.24	15.81±0.34
PM6+BTA3/ PY-IT	0.932	25.48	24.26	74.59	17.71
	0.931±0.002	25.24±0.35		74.35±0.19	17.43+0.25

[a] Obtained from the integration of the EQE spectrum.

Table S5. Photovoltaic parameters of PM6/PY-IT and PM6+BTA3/PY-IT solar cells with different thicknesses.

Active layer	Thickness (nm)	V_{oc} (V)	J_{sc} (mA·cm^{-2})	FF (%)	PCE (%)
PM6/PY-IT	70	0.918	24.76	71.47	16.24
	100	0.931	25.60	74.87	17.84
	200	0.914	24.59	71.13	15.99
	300	0.910	24.29	70.42	15.57
PM6+BTA3/PY-IT	70	0.933	25.40	75.47	17.88
	100	0.943	26.60	77.30	19.39
	200	0.925	25.92	72.90	17.48
	300	0.910	25.80	72.93	17.10

Table S6. Parameters used to extract the probabilities of exciton dissociation (P_{diss}) and charge collection (P_c).

Active layer	$J_{ph\cdot sat}$ (mA/cm^2)	$J_{ph.sc}$ (mA/cm^2)	$J_{ph.mpp}$ (mA/cm^2)	P_{Coll} (%)	P_{diss} (%)
PM6/PY-IT	25.64	25.19	22.22	0.982	0.867
PM6+BTA3/PY-IT	26.55	26.14	23.10	0.985	0.870

Table S7. Hole mobility (μ_h) and electron mobility (μ_e) of the PM6/PY-IT and PM6+BTA3/PY-IT all-PSCs.

Active layer	μ_h (10^{-4} cm^{2}Vs)	μ_e (10^{-4} cm^2/Vs)	μ_e/μ_h
PM6/PY-IT	3.32	4.03	1.21
PM6+BTA3/PY-IT	3.98	4.41	1.11

Table S8. Summarized photovoltaic parameters of PM6/PY-IT solar cells incorporated with various small molecule guests under AM 1.5G (100 mW·cm^{-2}) illumination (average PCE obtained from at least 10 devices).

Active layer	V_{oc} (V)	J_{sc} (mA·cm^{-2})	FF (%)	PCE (%)
PM6+PCBM/PY-IT	0.939 0.942±0.003	26.43 26.28±0.17	76. 46 76.13±0.34	18.98 18.93±0.22
PM6+ITIC/PY-IT	0.936 0.942±0.002	26.09 26.32±0.15	76.12 76.58±0.55	18.59 18.35±0.25
PM6+IT-4F/PY-IT	0.936 0.934±0.002	26.10 25.97±0.13	75.85 75.37±0.61	18.53 18.33±0.22
PM6+IT-M/PY-IT	0.931 0.930±0.003	25.99 25.97±0.10	76.13 76.03±0.25	18.42 18.33±0.31

Table S9. Summarized photovoltaic parameters of PM6/PY-DT and PM6/PY-FT solar cells incorporated with small molecule guest (BTA3) under AM 1.5G (100 mW·cm^{-2}) illumination (average PCE obtained from at least 10 devices).

Active layer	V_{oc} (V)	J_{sc} (mA·cm^{-2})	FF (%)	PCE (%)
PM6/PY-DT	0.945 0.943±0.002	24.55 24.28±0.17	74.00 73.83±0.34	16.92 16.43±0.42
PM6+BTA3/PY-DT	0.952 0.952±0.001	25.08 24.82±0.15	75.51 75.28±0.25	18.06 17.75±0.25
PM6/PY-FT	0.910 0.908±0.003	24.29 23.90±0.33	70.42 70.16±0.41	15.57 15.23±0.46
PM6+IT-M/PY-IT	0.931 0.930±0.003	25.30 24.97±0.38	71.38 71.03±0.32	16.58 16.35±0.21

Table S10. Contact angles (θ), surface energy (γ), and Flory-Huggins interaction parameters ($\chi_{donor-acceptor}$) determined based on the compounds of PCBM, PM6+ITIC, PM6+IT-4F and PM6+IT-M.

Material	θ_{Water} (deg.)	$\theta_{dilldomethane}$ (deg.)	γ (Mn m^{-1})	χ_{D-A}
PM6+PCBM	101.7	44.0	37.55	0.10
PM6+ITIC	101.2	43.5	37.81	0.09
PM6+IT-4F	101.0	45.5	36.77	0.15
PM6+IT-M	101.5	48.5	37.92	0.27